Panel-to-Substring Differential Power Processing Converter With Embedded Electrical Diagnosis Capability for Photovoltaic Panels Under Partial Shading

Masatoshi Uno, *Member, IEEE*, and Kazuma Honda

***Abstract*—Various kinds of differential power processing (DPP) converters have been developed to improve the energy yield of partially-shaded photovoltaic (PV) panels by precluding partial shading issues, such as the reduction in power generation and the occurrence of multiple maximum power points. Meanwhile, PV systems require fault diagnosis tools to detect premature deterioration and malfunctions that lead to a reduction in power generation of the system as a whole and, in the worst case, hazardous situations, such as a fire. This article proposes a novel DPP converter as well as an electrical diagnosis technique using the DPP converter. The proposed DPP converter not only addresses the partial shading issues but also provides the electrical diagnosis capability. In the diagnosis mode, the DPP converter injects ac currents to a panel, and an ac impedance of the panel can be calculated from the voltage response to the injected ac currents. The detailed operation analysis and experimental verification tests using a prototype were performed. The results demonstrated the improved power yield from partially shaded PV panels and the electrical diagnosis capability of the proposed DPP converter.**

***Index Terms*—AC impedance measurement, differential power processing (DPP) converter, partial shading, photovoltaic (PV) panel.**

I. Introduction

RENEWABLE energy sources have gained attention, and photovoltaic (PV) panels have been installed in various applications, such as residential rooftops, plug-in hybrid electric vehicles (PHEVs), and solar power plants. Each PV panel comprises multiple substrings connected in series, and the number of substrings varies depending on applications (e.g., three substrings in 60- and 72-cell standard PV panels, and seven substrings in solar roofs of Prius PHEVs [1]).

Partial shading on PV panels comprising multiple substrings connected in series is well known to trigger significantly reduced power generation. In an example case shown in Fig. 1(a), a shaded substring PV_1, which is less capable of generating current, is bypassed by a bypass diode connected in parallel. The bypassed substring no longer contributes to power generation as its voltage is subzero value, and therefore an extractable maximum power of the panel as a whole significantly decreases. For instance, 10% equivalent area of partial shading on a PV panel reportedly results in a 30% reduction in annual energy yield [2]. Similar characteristic-mismatch situations often happen in solar roofs of PHEVs due to the uneven irradiance on its curved surface [1], as illustrated in Fig. 1(b). Such characteristic mismatch due to partial shading or curved surfaces generate multiple maximum power points (MPPs), including a global MPP and local MPP(s), on a *P–V* characteristic of a panel [see Fig. 1(c)] and likely hinders and confuses ordinary MPP tracking algorithms.

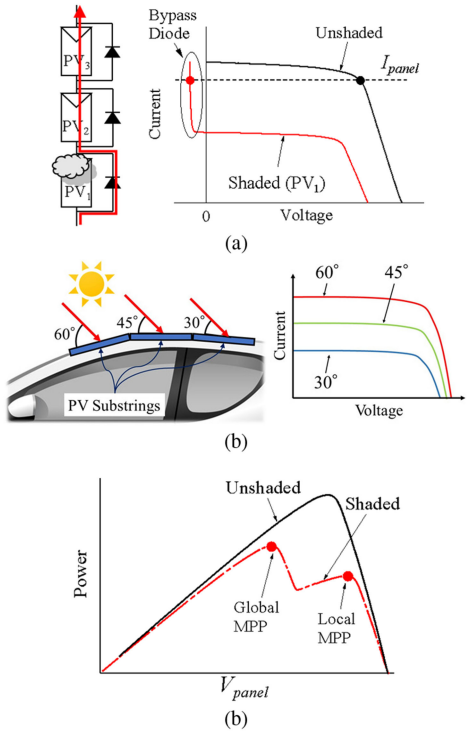

Fig. 1. (a) Mismatched substring characteristics due to partial shading. (b) Mismatched substring characteristics due to uneven irradiance on solar roofs. (c) Panel characteristics with/without partial shading.

Manuscript received October 25, 2020; revised January 17, 2021; accepted February 25, 2021. Date of publication March 9, 2021; date of current version June 1, 2021. This work was supported by Takahashi Industrial and Economic Research Foundation. Recommended for publication by Associate Editor O. Trescases. *(Corresponding author: Masatoshi Uno.)*

The authors are with the Graduate School of Science and Engineering, Ibaraki University, Hitachi 316-8511, Japan (e-mail: uno.m@mx.ibaraki.ac.jp; 19nm657y@vc.ibaraki.ac.jp).

Digital Object Identifier 10.1109/TPEL.2021.3064706

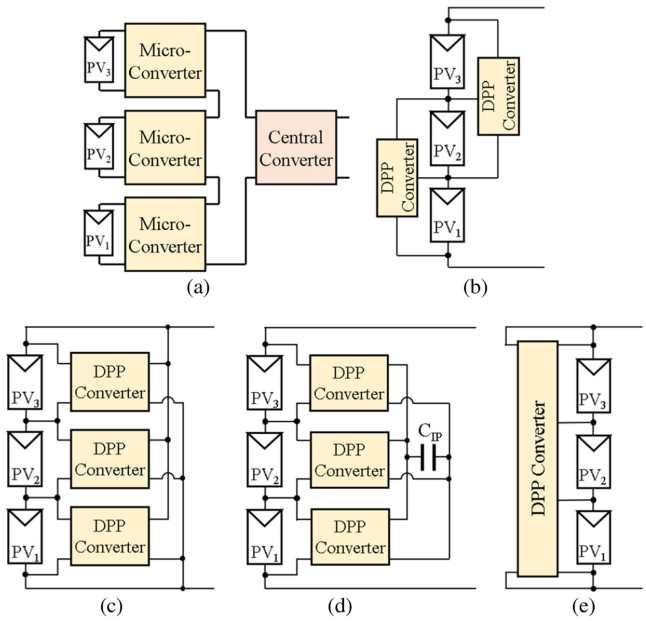

Fig. 2. Solutions to partial shading issues. (a) Distributed MPPT system. (b) DPP converters for adjacent substrings (PV-to-PV). (c) DPP converter for substring-to-bus. (d) DPP converter for substring-to-IP (virtual bus). (e) DPP converter for panel-to-substring architecture.

To cope with the partial shading issues, a variety of solutions to partial shading have been proposed and developed, as shown in Fig. 2. With distributed MPPT systems using micro-converters [3], [4], also known as dc optimizers, all PV substrings can operate at each MPP, regardless of characteristic mismatch due to partial shading. However, since as many converters as the number of substrings are necessary, the complexity and cost of the system are prone to soar. Furthermore, micro-converters in the distributed MPPT systems are essentially a full power processing (FPP) converter that handles the full power of each substring. The power rating, cost, and loss of FPP converters are unavoidably larger than those of differential power processing (DPP) converters.

Various kinds of DPP converters or voltage equalizers have been proposed and developed to address partial shading issues [5]–[35]. The DPP converters transfer a fraction of the generated power of unshaded substrings to shaded ones so that all substring characteristics are virtually unified, thus the partial shading issues can be precluded. Since the DPP converters deal with only differential power between unshaded and shaded substrings, not only can the overall system efficiency be improved but also the power rating of DPP converters can be reduced in comparison with conventional FPP converters.

The DPP converters are roughly categorized into architectures shown in Figs. 2(b)–(e). In the adjacent substring-to-substring architecture [see Fig. 2(b)], nonisolated bidirectional converters, such as PWM converters [6]–[12], multistage choppers [13], [14], and switched capacitor converters [15]–[22], are employed to transfer power between neighboring substrings. The numbers of DPP converters as well as switches are proportional to the number of substrings connected in series, likely increasing the system complexity and cost. Furthermore, collective power conversion loss due to multiple power conversion stages is also a concern as power from unshaded substrings may have to traverse several DPP converters before reaching shaded substrings—power transfer in this architecture is limited only between neighboring substrings.

The issue of the collective power conversion loss can be resolved by the architecture shown in Fig. 2(c) [23]–[29]. DPP converters in these architectures are a bidirectional isolated flyback converter that allows direct power transfer between a substring and panel. With an isolated port (IP) [see Fig. 2(d)], direct power transfer between substrings via the IP is feasible. Although flexible power redistribution is feasible in these architectures, numerous isolated bidirectional converters in proportion to the number of substrings are necessary, posing issues of increased cost and complexity.

The panel-to-substring DPP converter based on a single-input–multioutput converter [30]–[35], shown in Fig. 2(e), is the simplest solution. Not only can the number of DPP converters be reduced to only one, but also the DPP converter can be a nonisolated topology without a bulky isolation transformer. The panel-to-substring DPP converter generally behaves as a voltage equalizer, and therefore, individual MPPT control is no longer feasible. However, an energy yield loss due to the voltage equalization, in comparison with the individual MPPT control, is reportedly only a few percent [10], [26], and therefore, equalizing substring voltages simply is considered sufficient in most applications.

Meanwhile, PV systems comprise numerous panels, depending on applications—several to dozen panels on residential rooftops, and more than a thousand panels in solar power plants. Panel characteristics are unavoidably mismatched to some extent due to manufacturing tolerance, uneven aging, electrical or mechanical damages, and unexpected malfunctions. Such situations would reduce the energy yield of the system as a whole and, in the worst case, reportedly trigger a catastrophic fire hazard.

In order to operate PV systems efficiently and safely, panels are desirably diagnosed to detect premature deterioration and malfunctions, and therefore, PV systems require fault diagnosis tools. Conventional fault diagnosis techniques using an *I–V* curve tracer or thermal camera, however, incur high costs due to maintenance personnel and expensive instruments. An electrical diagnosis technique capable of an autonomous diagnosis based on ac impedance spectroscopy is a promising solution [36]–[38]. An ac impedance characteristic of a panel is measured from a voltage response to an injected ac current is often expressed in the form of Nyquist plot, which provides a visual representation of complex ac impedance characteristics, as illustrated in Fig. 3. Shapes of Nyquist plots vary depending on panels' internal parameters, such as series- and parallel-resistances (R_s and R_p) and diffusion capacitance (C_d) [21], [36], [37], and the existence of hot spots as well [38]. However, Nyquist plots are generally measured using expensive benchtop equipment, such as frequency response analyzer (FRA) and impedance analyzer.

The spectroscopic diagnosis capability can be embedded in switching converters, and several online impedance measurement techniques have been proposed for rechargeable batteries

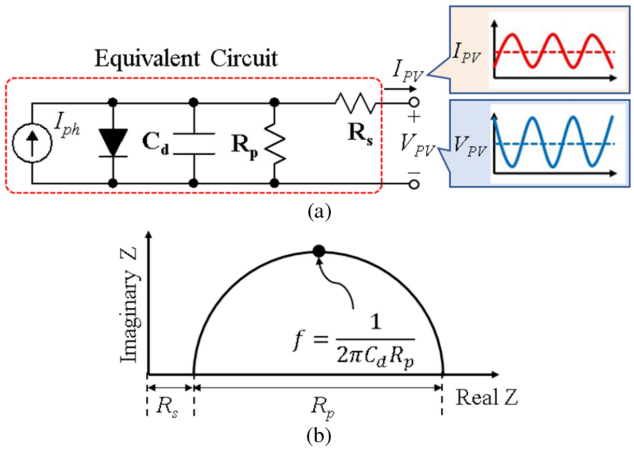

Fig. 3. (a) Equivalent circuit of PV substring. (b) Typical Nyquist plot of PV substring.

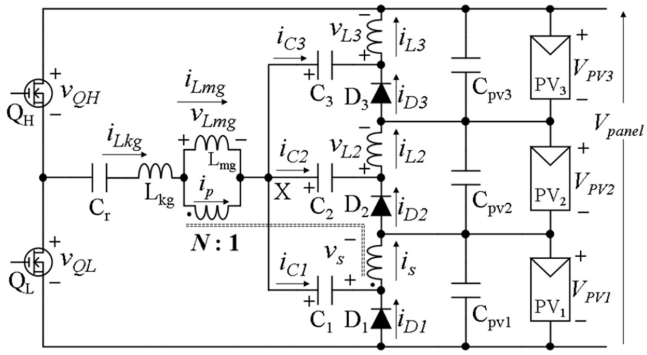

Fig. 4. Proposed panel-to-substring DPP converter for three substrings.

and fuel cells [39]–[44]. Main converters, such as a battery charger and motor driver, perturb electrochemical operating states of batteries by injecting ac currents [39]–[42]. The fault diagnosis technique using a converter for PV panels in the distributed MPPT systems has also been proposed [45]. However, the input and output currents of the main converters unavoidably fluctuate to some extent during the online impedance measurement, likely affecting the system operation. Battery cell equalizers with the embedded spectroscopic diagnosis capability have also been developed as an alternative solution [43], [44]. Cell impedances can be individually measured without perturbating a whole string current, thus unaffecting the system operation. These techniques, however, rely on adjacent cell-to-cell equalizers that are identical to the adjacent substring-to-substring DPP converter architecture in Fig. 2(b), with which the system complexity, cost, and collective power conversion loss are prone to soar, as aforementioned.

This article proposes a novel panel-to-substring DPP converter and its electrical diagnosis technique. The proposed DPP converter can not only preclude the partial shading issues but also provide the electrical diagnosis capability. The proposed DPP converter operates either in the equalization mode or diagnosis mode. In the equalization mode, the DPP converter nearly equalizes substring voltages by supplying equalization currents to shaded substrings. In the diagnosis mode, the DPP converter injects ac equalization currents to all substrings in order to perturb substring currents, and ac impedances of substrings can be determined from the voltage responses to perturbed substring currents. The past works have reported a variety of signal processing and impedance estimation techniques, such as single-sine frequency sweep, multisine excitation with Fourier transforms, modified particle swarm optimization, etc. [40], [42], [45], and therefore, this article focuses only on producing ac equalization currents by the proposed panel-to-substring DPP converter so that substring currents are perturbed.

The rest of this article is organized as follows. Section II introduces the proposed panel-to-substring DPP converter and its major features. Section III presents the operation analysis for the proposed converter. Section IV discusses the control strategies for the equalization and diagnosis modes. The experimental results of equalization and diagnosis tests using a prototype for three substrings will be presented in Section V. Finally, Section VI concludes the article.

II. Proposed Panel-to-Substring DPP Converter

A. Circuit Description

The proposed panel-to-substring DPP converter for three substrings (PV_1–PV_3) is shown in Fig. 4. This DPP converter operates as a quasi-resonant tapped-inductor (TI) PWM step-down converter. The input port is the switching leg Q_H–Q_L, while there are three output ports of smoothing capacitors C_{pv1}–C_{pv3}. The leakage inductance L_{kg} and the resonant capacitor C_r form a series-resonant tank.

The series connection of PV_1–PV_3 is tied to the input of the DPP converter, and therefore, a fraction of the generated power of the panel is fed to the DPP converter. The DPP converter produces three uniform output voltages across C_{pv1}–C_{pv3}, automatically equalizing the voltages of PV_1–PV_3, V_{PV1}–V_{PV3}. The output voltages are dependent on the duty cycle of switches, allowing an ac current injection to substrings by sinusoidally varying the duty cycle.

B. Features

The proposed DPP converter belongs to the panel-to-substring DPP converter architecture and can handle multiple substrings at a time. Furthermore, the switch count is only two, regardless of the number of series-connected substrings. Thus, the proposed DPP converter realizes the simplified system and circuit by reducing the numbers of DPP converters and switches in comparison with conventional topologies.

Switches in the proposed DPP converter must withstand the full input voltage. Ordinary panel voltages are within several ten volts, and low-voltage rating MOSFETs can be used. In high-voltage large string applications, since the input voltage reaches several hundred volts, the proposed DPP converter is not suitable for such large string applications.

Some conventional panel-to-substring DPP converters also offer a simple circuit and duty-dependent voltage conversion as

TABLE I
COMPARISON BETWEEN PROPOSED AND CONVENTIONAL DPP CONVERTERS

Topology	Architecutre	Switch	L	C†	D	Transformer or TI	Conversion Ratio
Bidirectional PWM Converter [6]–[11]	Adjacent Substrings	$2(n-1)$	$n-1$	-	-	-	$d/(1-d)$
Switched Capacitor Converter [15], [19], [20]	Adjacent Substrings	$2n$	-	$n-1$	-	-	1
Flyback Converter [23], [28], [29]	Substring-to-Bus	$2n$	-	-	-	n	$d/N(1-d)$
Flyback Converter [23]–[25], [27]	Substring-to-IP	$2n$	-	1	-	n	$d/N(1-d)$
Multi-Stacked Buck-Boost Converter [31], [32]	Panel-to-Substring	1	$n+1$	n	n	-	$d/(1-d)$
LLC Resonant Voltage Multiplier [33]	Panel-to-Substring	2	-	$n+1$	$2n$	1	$1/N$
Proposed	Panel-to-Substring	2	$n-1$	$n+1$	n	1 (TI)	$d/(N+1)$

†Smoothing capacitors excluded

their topologies are based on buck-boost converters [31], [32], but their duty cycles might be extremely low for PV panels containing a large number of substrings (e.g., seven substrings in Prius PHEVs' solar roofs), as will be discussed in Section II-C. On the other hand, the voltage conversion ratio of the proposed DPP converter is dependent on not only the duty cycle but also the turn ratio of the TI, allowing a more flexible design.

The proposed DPP converter also offers the electrical diagnosis capability for PV panels. The DPP converter injects ac currents to all substrings to perturb substring currents, and ac impedances of substrings are measured from the voltage responses. PV panels would be diagnosed without dedicated diagnosis tools, such as *I–V* curve tracer, thermal camera, and FRA, realizing low-cost diagnosis of PV panels.

The proposed DPP converter is a single-input–multioutput converter that equalizes substring voltages by outputting the same voltages to all substrings. The voltage equalization is only applicable to panels whose substrings comprise the same number of cells connected in series. In other words, if the number of cells in each substring differs, the proposed DPP converter cannot be employed. However, substring structures in an ordinary PV panel are identical and do not differ (e.g., standard 72-cell panels consist of three 24-cell substrings), and therefore the proposed DPP converter can be applied to most PV panels.

C. Comparison With Conventional DPP Converters

The proposed and conventional DPP converters are quantitatively compared from the viewpoints of the component counts and voltage conversion ratio, as shown in Table I. n is the number of substrings in a panel, and N is the turn ratio of transformers or TIs. The switch count can be a good index to represent the circuit complexity as every one or two switches require a gate driver circuit, including a gate driver IC and its auxiliary power supply. The numbers of magnetic components imply the circuit volume as they are the bulkiest circuit components in low-voltage dc–dc converters.

Conventional DPP converters based on the adjacent substring-to-substring [6]–[11] or substring-to-bus architectures [23]–[29] require numerous switches in proportion to n. DPP converters based on flyback converters also require n transformers. On the other hand, the panel-to-substring DPP converters [31]–[33], including the proposed topology, can significantly reduce the switch count, achieving the simplified circuit.

The switched capacitor converter [15], [19], [20], and LLC resonant voltage multiplier [33] cannot be used for the impedance measurement because their voltage conversion ratios are essentially constant and not controllable. Topologies with duty-dependent voltage conversion ratios can potentially be used for the electrical diagnosis based on the ac impedance measurement. The multistacked buck-boost converter [31], [32] is a single-switch topology with a duty-dependent voltage conversion ratio, but its duty cycle d tends to be extremely low for PV panels comprising a large number of substrings. For solar roofs consisting of seven substrings, for example, the voltage conversion ratio is 1/7, and therefore, $d = 0.125$. Given the duty cycle perturbation during the ac impedance measurement, d would momentarily be even smaller.

The voltage conversion ratio of the proposed DPP converter, on the other hand, is adjustable with N. Hence, the proposed DPP converter can be applied to any number of series-connected substrings, without suffering from the extreme duty cycle operations, by properly designing N.

III. OPERATION ANALYSIS

A. Voltage Equalization Mechanism

The proposed DPP converter produces the uniform output voltages (i.e., voltages of C_{pv1}–C_{pv3}), as mentioned in Section II. The equivalent circuit, shown in Fig. 5, explains the voltage equalization mechanism. A square wave voltage is generated at the node X (see Fig. 4), at which coupling capacitors C_1–C_3 are connected. This suggests that dc voltages of C_{pv1}–C_{pv3} or V_{PV1}–V_{PV3} can be separated and grounded, as shown in Fig. 5. Although the secondary winding of the TI is connected to C_{pv1}, all the *C-D-L* circuits as well as substrings are equivalently connected in parallel.

A voltage of a shaded substring is lower than others under partial shading conditions. In such a case, a current from the square wave voltage source v_x preferentially flows toward the shaded substring having the lowest voltage in the panel. The voltage of the shaded substring is boosted by the equalization current supplied from the DPP converter.

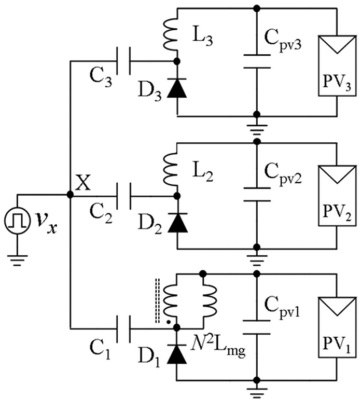

Fig. 5. Equivalent circuit of the proposed DPP converter.

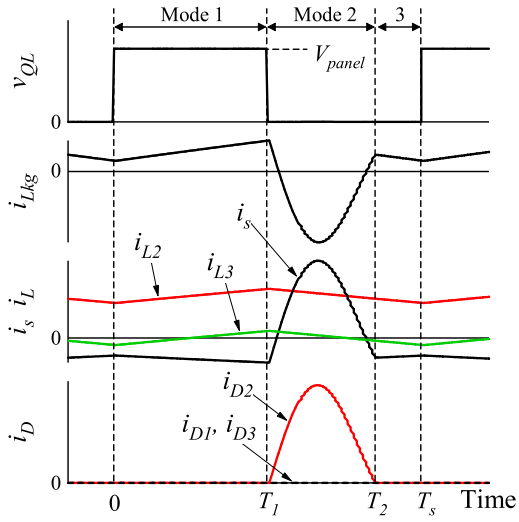

Fig. 6. Theoretical key operation waveforms when PV_2 is partially shaded.

B. Operation Mode

Shading patterns vary depending on time, seasons, locations, etc. This section deals with a representative case that PV_2 only is shaded. However, other shading conditions can be analyzed similarly.

All circuit elements are assumed ideal, and resistive components and diode forward voltage drops are neglected unless otherwise noted. The magnetizing inductance of the TI, L_{mg}, is assumed rather larger than the leakage inductance L_{kg} (i.e., $L_{mg} >> L_{kg}$), and the voltage across L_{kg} is neglected to simplify equations. The duty cycle of Q_H is d, and the average voltage at the node X is defined as V_X.

Before detailing operation modes, average voltages of C_r and C_1–C_3 (V_{Cr} and V_{C1}–V_{C3}) are determined. The average voltage at the switching node is equal to dV_{panel}. Meanwhile, average voltages at the cathode pins of D_1, D_2, and D_3 are V_{PV}, $2V_{PV}$, and V_{panel} ($= 3V_{PV}$), respectively. Hence, V_{Cr} and V_{C1}–V_{C3} are yielded as

$$V_{Cr} = dV_{\text{panel}} - V_X \tag{1}$$

$$\begin{cases} V_{C1} = V_X - V_{PV1} \\ V_{C2} = V_X - (V_{PV1} + V_{PV2}) \\ V_{C3} = V_X - V_{\text{panel}}. \end{cases} \tag{2}$$

The theoretical key operation waveforms and current flow directions are shown in Figs. 6 and 7, respectively.

Mode 1 ($0 \le t < T_1$) [see Fig. 7(a)]: Q_H is turned ON. The voltage of Q_L, v_{QL}, becomes V_{panel}. All diodes are reverse-biased and are not conducting. Since all the diodes are OFF, the current paths in Fig. 7(a) yields the current of L_{kg}, i_{Lkg}, as

$$i_{Lkg} = i_p + i_{Lmg} = i_s + i_{L2} + i_{L3} = -Ni_p + i_{L2} + i_{L3}$$
$$\rightarrow i_{Lkg} = \frac{Ni_{Lmg} + i_{L2} + i_{L3}}{1+N} \tag{3}$$

where i_p and i_s are the primary and secondary winding current, respectively, i_{Lmg} is the magnetizing inductance current, and i_{L2} and i_{L3} are the currents of L_2 and L_3, respectively.

The voltage applied to L_{mg}, v_{Lmg}, can be yielded from the current path of C_r, TI, and C_1 with (1) and (2), as

$$v_{Lmg} = \frac{N}{N+1}\left(V_{\text{panel}} - V_{Cr} - V_{C1} - V_{PV1}\right) = \frac{(1-d)\,NV_{\text{panel}}}{N+1} = Nv_s \tag{4}$$

where v_s is the voltage of the TI's secondary winding (see Fig. 4). The voltages applied to L_2 and L_3, v_{L2} and v_{L3}, are

$$v_{L2} = V_{\text{panel}} - V_{Cr} - v_{Lmg} - V_{C2} - (V_{PV1} + V_{PV2}) = \frac{(1-d)\,V_{\text{panel}}}{N+1} \tag{5}$$

$$v_{L3} = V_{\text{panel}} - V_{Cr} - v_{Lmg} - V_{C3} - V_{\text{panel}} = \frac{(1-d)\,V_{\text{panel}}}{N+1}. \tag{6}$$

These equations suggest that v_s, v_{L2}, and v_{L3} are expressed in identical form even though their positions differ.

Mode 2 ($T_1 \le t < T_2$) [see Fig. 7(b)]: Q_L is turned ON. L_{kg} and C_r start resonating, and i_{Lkg} flows through D_2 and C_2. i_{Lkg} in this mode is expressed as

$$i_{Lkg}(t) = \frac{-NV_{PV}}{|Z_0|}\, e^{-\gamma(t-T_1)} \sin\omega_r (t-T_1) + i_{Lkg}(T_1) \tag{7}$$

where Z_0 is the characteristic impedance of the resonant tank, γ is the damping factor, and ω_r is the damped resonant angular frequency. Z_0, γ, and ω_r are given by

$$Z_0 = \sqrt{\frac{L_{kg}}{C_r}},\quad \gamma = \frac{R}{2L_{kg}},\quad \omega_r = \sqrt{\frac{1}{L_{kg}C_r} - \gamma^2} \tag{8}$$

where R is the total resistance of the resonant current path.

Since the diode D_2 conducts, L_2 is connected in parallel with PV_2. Meanwhile, other diodes are still OFF. v_s, v_{L2}, and v_{L3} are

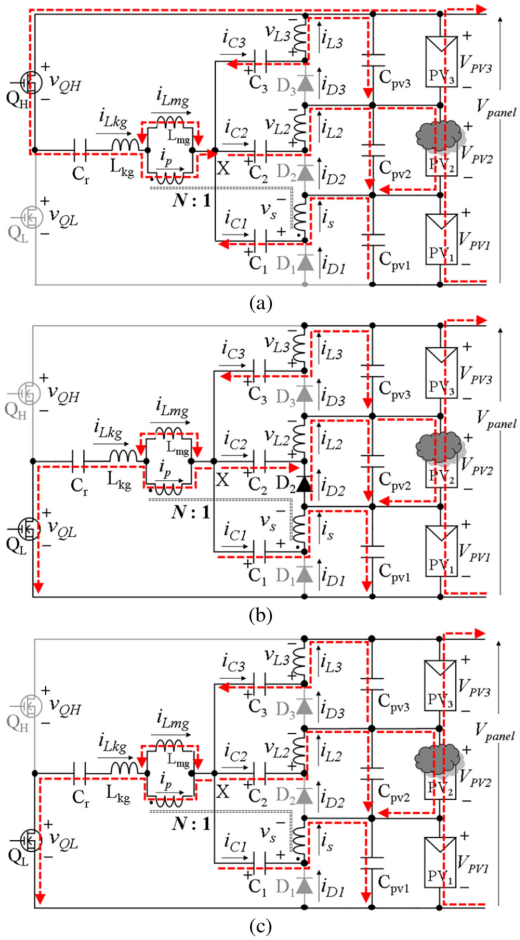

Fig. 7. Current flow path in Mode (a) 1, (b) 2, and (c) 3 when PV_2 is partially shaded.

expressed as

$$v_s = -V_{C1} + V_{C2} = v_{L2} \tag{9}$$

$$v_{L2} = -V_{PV2} \tag{10}$$

$$v_{L3} = V_{C2} - V_{C3} + v_{L2} - V_{PV3} = v_{L2}. \tag{11}$$

Mode 3 ($T_2 \le t < T_s$) [see Fig. 7(c)]: D_2 ceases to conduct, while other current flow paths are identical to those in the previous mode. According to the current flow paths, v_s and v_{L3} in this mode are also identical to those in Mode 2, yielding

$$v_s = v_{L2} = v_{L3} = -V_{PV2}. \tag{12}$$

In summary, D_2 conducts, whereas other diodes are OFF for the entire period. Average currents of C_1–C_3 under steady-state conditions must be zero, and therefore, average diode currents are equal to average inductor currents or equalization currents supplied to substrings. In other words, the average current of i_{D2} equals the average of i_{L2} as well as the equalization current I_{eq} for PV_2. On the other hand, since no current flows through D_1 and D_3, the average current of the secondary winding i_s and i_{L3} are zero, and therefore no equalization current flows toward PV_1 and PV_3.

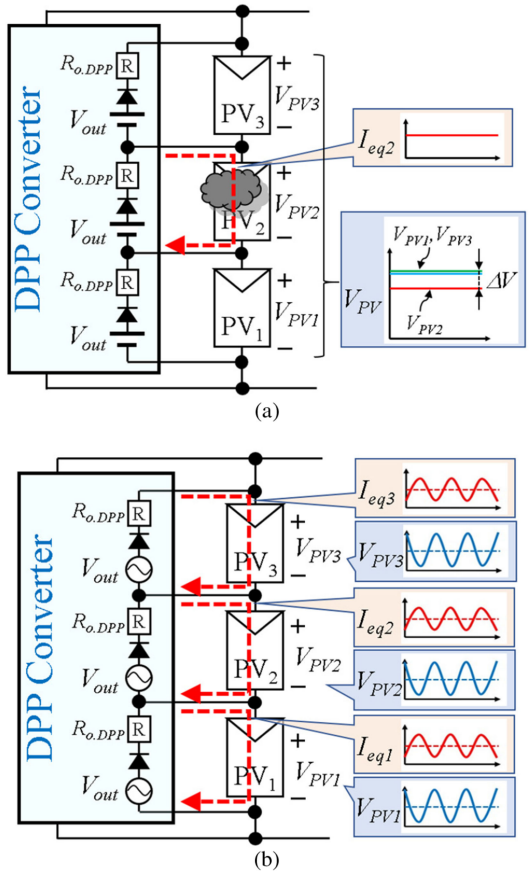

Fig. 8. Operation mode of proposed panel-to-substring DPP converter. (a) Equalization mode (ΔV-controlled equalization). (b) Diagnosis mode (ac impedance measurement mode).

C. Voltage Conversion Ratio

From the volt–sec balance on L_2, the voltage conversion ratio can be yielded from (5), (10), and (12), as

$$V_{PV2} = \frac{1}{N+1}\, dV_{\text{panel}}. \tag{13}$$

This equation suggests that the voltage of shaded substring (V_{PV2}) can be regulated by PWM control manipulating d. Properly designing N can avoid extreme duty cycle operations even for applications with a low value of V_{PV}/V_{panel}, such as PHEV solar roofs.

Equation (13) can be generalized as

$$V_{\text{out}} = \frac{1}{N+1}\, dV_{\text{panel}} \tag{14}$$

where V_{out} is the output voltage of the proposed DPP converter. This equation can be applied to any shading conditions even when multiple substrings are partially shaded simultaneously.

IV. Control Strategy

The proposed DPP converter operates either in the equalization mode or diagnosis mode. Fig. 8 illustrates the operational images in these two modes. In the equalization mode [see Fig. 8(a)], the DPP converter provides equalization current(s)

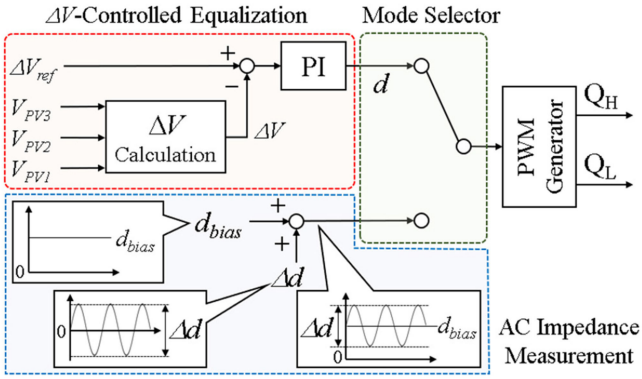

Fig. 9. Control block diagram.

to shaded substrings, whereas no current flows toward unshaded ones. In the diagnosis mode [see Fig. 8(b)], on the other hand, the DPP converter feeds all substrings with equalization currents containing ac components.

A. Mode Selection

The control block diagram for the proposed DPP converter is shown in Fig. 9. The equalization and diagnosis modes can be selected by the mode selector, and these two modes do not take place simultaneously.

In general, irradiance and shading conditions change relatively fast, whereas the state of health of PV panels gradually degrades. Hence, the DPP converter should operate with the equalization mode most of the time to preclude partial shading issues. Meanwhile, the diagnosis mode is occasionally activated—diagnosing once a day or even once a week would be frequent enough to grasp degradation trends of PV panels. The energy yield from the PV panel cannot be maximized during the diagnosis mode. However, since the ac measurement can be completed in a few minutes, the occasional diagnosis does not impair the daily energy yield.

B. ΔV-Controlled Equalization Mode

The DPP converter desirably supplies equalization currents to only shaded substring(s) in order to minimize the processed power as well as power conversion losses in the converter. To this end, the current sensorless ΔV-controlled equalization strategy has been proposed [32]. Panel-to-substring DPP converters behave as a single-input–multioutput converter producing uniform output voltages $V_{\rm out}$, as illustrated in Fig. 8(a). In order to provide equalization currents to shaded substrings only, the relationship between the unshaded and shaded substring voltages, $V_{\rm unshaded}$ and $V_{\rm shaded}$, must meet $V_{\rm unshaded} > V_{\rm out} > V_{\rm shaded}$—in the case of Fig. 8(a), $V_{\rm unshaded} = V_{PV1} = V_{PV3}$ and $V_{\rm shaded} = V_{PV2}$. Given a voltage drop across an equivalent output resistance $R_{o.DPP}$ of the DPP converter, $V_{\rm out}$ is expressed as

$$V_{\rm unshaded} > V_{\rm out} = I_{eq}\, R_{o.DPP} + V_{\rm shaded}. \qquad (15)$$

Rearrangement of (15) produces

$$\Delta V = V_{\rm unshaded} - V_{\rm shaded} > I_{eq} R_{o.DPP} \qquad (16)$$

where ΔV is the voltage difference between the unshaded and shaded substrings. This equation suggests that ΔV should be greater than the voltage drop across $R_{o.DPP}$ even when the largest I_{eq} flows.

In the control block, all substring voltages, V_{PV1}–V_{PV3}, are individually measured, followed by the ΔV calculation. ΔV is regulated to be $\Delta V_{\rm ref}$ by manipulating d. The value of $\Delta V_{\rm ref}$ should be determined with considering the largest I_{eq} in the worst case. Previous works suggest that DPP converters with a power rating of 20%–30% of a panel power are sufficient in most cases [46], [47]. Accordingly, $\Delta V_{\rm ref}$ should be determined to fulfill (16) even when I_{eq} is equal to 20%–30% of a short-circuit current of unshaded substrings.

C. Diagnosis Mode

The DPP converter behaves as a multioutput ac voltage source, as illustrated in Fig. 8(b), to generate an equalization current containing ac components. Substrings' ac impedances can be measured from the injected ac currents and voltage responses. To this end, d needs to be perturbed sinusoidally by superimposing sinusoidal duty cycle variation Δd to a dc bias duty cycle $d_{\rm bias}$, as shown in Fig. 9. Equalization currents must flow toward all substrings even during duty cycle perturbation. In other words, the output voltage of the DPP converter with the lowest instantaneous value of $d = d_{\rm bias} - \Delta d/2$ must exceed the voltage of unshaded substrings, $V_{\rm unshaded}$. Rearrangement of (14) yields the following relationship:

$$d_{\rm bias} - \frac{\Delta d}{2} > (N+1)\,\frac{V_{\rm unshaded}}{V_{\rm panel}} \qquad (17)$$

where $d_{\rm bias}$ dictates the dc current component of equalization currents that is unnecessary information in the ac impedance measurement. Hence, $d_{\rm bias}$ should be as small as possible, but without violating (17), to minimize the dc current components as well as associated losses in the DPP converter. Meanwhile, Δd directly links to ac current and voltage components. Since the characteristics of PV panels are nonlinear, voltage perturbation for PV panels should be as small as possible. Amplitudes of voltage perturbation for single PV cells in laboratory tests using dedicated equipment are around 10 mV [36], [37]. On the other hand, online impedance measurement using switching converters would necessitate larger perturbation amplitude because of the noisy environment due to switching operations of converters. In general, an amplitude of voltage perturbation is empirically determined depending on the characteristics of a device under test. In our experiment, Δd of the proposed DPP converter was empirically determined to be 0.05 based on (14) so that the perturbation amplitude was about several hundred millivolts for substrings at $V_{\rm panel}$ of 30–36 V—this condition is equivalent to that the perturbation amplitude of several ten millivolts for single cells in each substring.

The ac impedance measurement using benchtop equipment is generally carried out in a frequency range exceeding 100

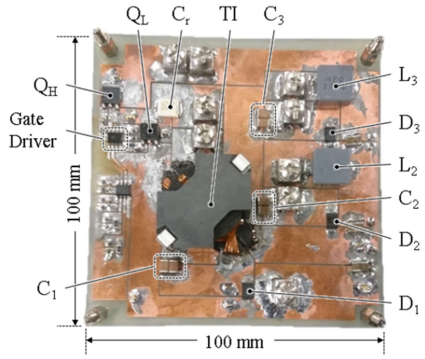

Fig. 10. Prototype of proposed panel-to-substring DPP converter for three substrings.

kHz [36]–[38]. On the other hand, a frequency range of the ac impedance measurement using the DPP converter can never exceed the converter's switching frequency f_s. The ac impedance measurement frequency range should be up to around one-tenth of f_s—if f_s is 100 kHz, the measurement frequency should be lower than around 10 kHz. Such a frequency range would be high enough in practical diagnosis cases because a whole semi-circle of Nyquist plot can be obtained in a frequency range lower than several kilohertz, as will be demonstrated in Section V-D. The sampling frequency in the diagnosis mode is equal to the switching frequency.

Nyquist plots can be obtained by processing the measured ac currents and voltage responses. Various kinds of signal processing and impedance estimation techniques, such as single-since frequency sweep, multisine excitation with Fourier transforms, etc. [39]–[44], have been proposed in the past works, and therefore, this article does not deal with the signal processing during the ac impedance measurement. In the next section, experimental verification tests will be performed focusing on perturbing currents by the DPP converter, not the signal processing to derive Nyquist plots.

V. Experimental Results

A. Prototype

A prototype of the proposed panel-to-substring DPP converter that can supply 24 W for each shaded substring was built for three substrings connected in series, as shown in Fig. 10. Component values are listed in Table II. The prototype was operated at a switching frequency of 100 kHz.

B. Efficiency and Output Characteristics of DPP Converter

The experimental setup shown in Fig. 11 was used to measure the power conversion efficiency and output characteristics of the prototype. Substrings PV_1–PV_3 were removed, and a variable resistor $R_{\rm var}$ was connected to either $C_{\rm pv1}$–$C_{\rm pv3}$ via selectable taps S_1–S_3 to emulate current flow paths under partial shading conditions. Closing S_2, for example, emulates the current flow paths in the PV_2-shaded condition. In this setup, $I_{\rm out}$ corresponds to the equalization current I_{eq}. The experiments were performed with $d = 0.5$ and an external power supply with $V_{in} = 36$ V, which was equivalent to the MPP voltage of a panel.

TABLE II
Component List of DPP Converter Prototype

Component	Value
Q_1, Q_2	FDD390N15A, R_{on} = 35.5 mΩ
C_r	Film Capacitor, 470 nF
C_1–C_3	Ceramic Capacitor, 44 μF
C_{pv1}–C_{pv3}	Ceramic Capacitor, 200 μF
Tapped Inductor	N_1:N_2 = 10:20, L_{kg} = 1.0 μH, L_{mg} = 52 μH
L_2, L_3	47 μF
D_1–D_3	Schottky Diode, SBRT20M60SP5, V_f = 0.43 V

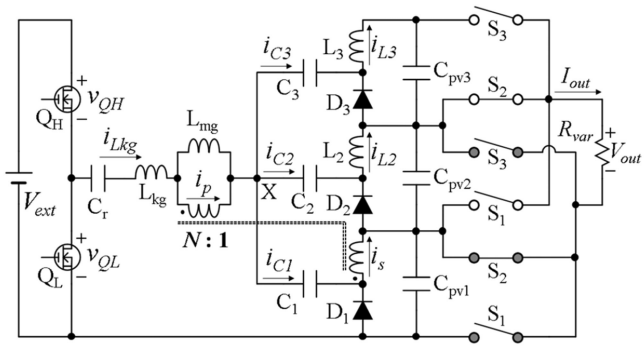

Fig. 11. Experimental setup for characteristic measurement.

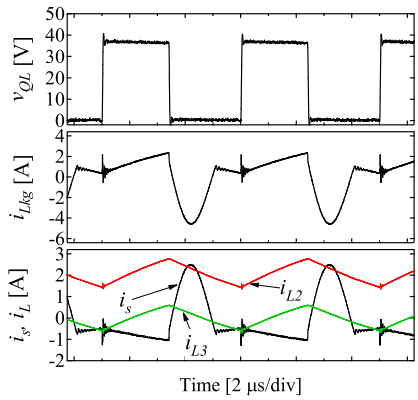

Fig. 12. Measured waveforms when $I_{\rm out} = 2.0$ A.

Measured key waveforms at $I_{\rm out} = 2.0$ A in the PV_2-shaded condition are shown in Fig. 12. Average currents of i_s and i_{L3} were zero, while that of i_{L2} was substantial, as discussed in Section III-B. These waveforms agreed well with the theoretical ones shown in Fig. 6, verifying the operation of the prototype.

The measured power conversion efficiency and output characteristics are shown in Fig. 13. From the measured output *I–V* characteristic, the equivalent output resistance $R_{o.DPP}$ was calculated to be 0.65 Ω. The average power conversion efficiencies in the range of $I_{\rm out}$ greater than 0.5 A were 92%. The measured average efficiency is comparable to that of conventional panel-to-substring DPP converters (ca. 90% [31], [32] and 92%–93% [33]).

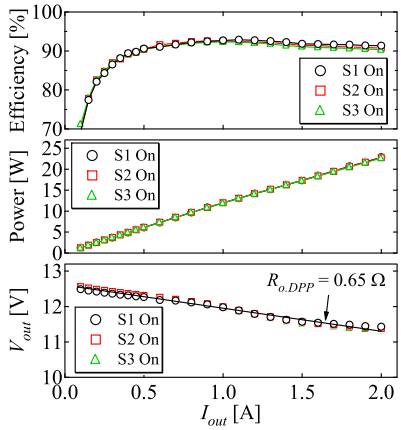

Fig. 13. Measured characteristics.

C. Equalization Mode

Two sets of experimental equalization tests emulating partial shading conditions were performed using solar array simulators (E4361A, Keysight Technologies). Individual substring characteristics used in Case 1 are shown in Fig. 14(a). PV_2 was severely shaded and its short-circuit current was 3.5 A, which was 1.5 A lower than those of unshaded substrings—PV_2 was approximately 30% less capable of producing power. The sum of maximum powers of all substrings in Case 1 was 147 W. The DPP converter operated with the ΔV-controlled equalization strategy. Based on (16) and the calculated $R_{o.DPP}$ from Fig. 13(b), ΔV was determined to be 1.0 V ($\approx$1.5 A $\times$ 0.65 Ω) by assuming the largest equalization current of $I_{eq} = 1.5$ A. Panel characteristics were manually swept using an electronic load.

The measured panel characteristics with/without the DPP converter in Case 1 are compared in Fig. 14(b). There were two MPPs observed on the *P–V* characteristic without the DPP converter, and the maximum power at the global MPP was 122 W. With the DPP converter, on the other hand, the local MPP disappeared, and the maximum power increased to as high as 143 W, corresponding to 17.2% improvement in power yield and the overall efficiency of 97.3% (=143/147 W).

Individual substring characteristics during the equalization mode are shown in Fig. 14(c). The DPP converter nearly unified the substring characteristics, but the voltage of PV_2 was approximately 1 V lower than others due to the ΔV-controlled equalization.

Another test was also performed under different shading conditions. As shown in Fig. 15(a), Case 2 emulated that PV_1 and PV_3 were simultaneously shaded, but their characteristics differed. The ideal maximum power of the panel as a whole was 148 W in Case 2.

The measured panel characteristics in Case 2 are shown in Fig. 15(b). The *P–V* characteristic without the DPP converter exhibited one global and two local MPPs, and the maximum power at the global MPP was 136 W. The DPP converter eliminated the local MPPs and increased the maximum power as high as 142 W. The results correspond to 4.4% improvement in power generation and the overall efficiency of 95.9% (= 142/148 W).

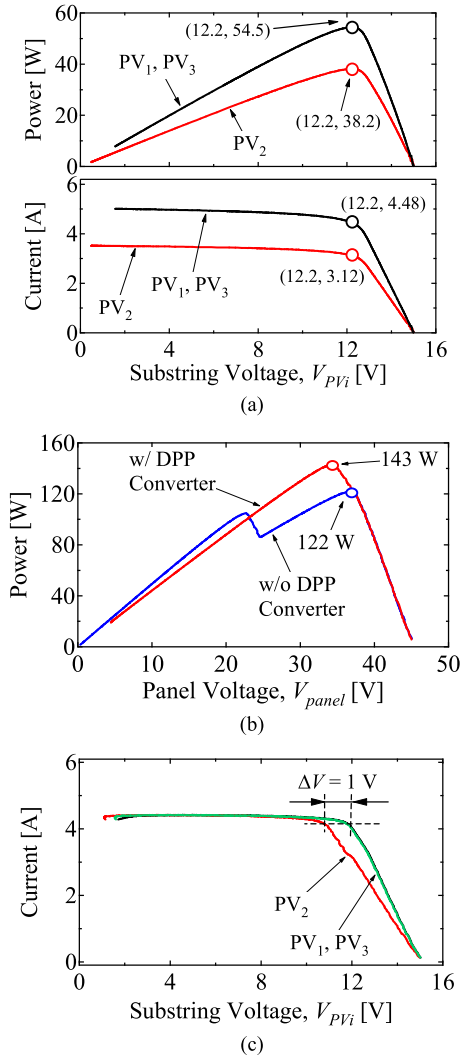

Fig. 14. Experimental results of equalization mode in Case 1. (a) Individual substring characteristics used for the experiment. (b) Measured panel characteristics with/without DPP converter. (c) Substring characteristics equalized by DPP converter.

Individual substring characteristics during the equalization test in Case 2 are shown in Fig. 15(c). Similar to Case 1, all substring voltages were nearly unified by the DPP converter. The voltage of PV_1, which was the most shaded substring in this case, was 1 V lower than that of the unshaded PV_2.

D. Diagnosis Mode

Internal circuit parameters of actual PV panels are strongly dependent on time-varying irradiance level, temperature, and bias voltage [21], [36]–[38]. To demonstrate the efficacy of the proposed DPP converter's diagnosis capability, the reproducibility of PV panel characteristics must be ensured. Solar array simulators are a good tool to emulate dc characteristics but are not suitable to emulate dynamic characteristics that are characterized by the series and parallel resistances (R_s and R_p) and diffusion capacitance C_d.

To facilitate experiments in the diagnosis mode in the laboratory, PV substring emulators based on the equivalent circuit

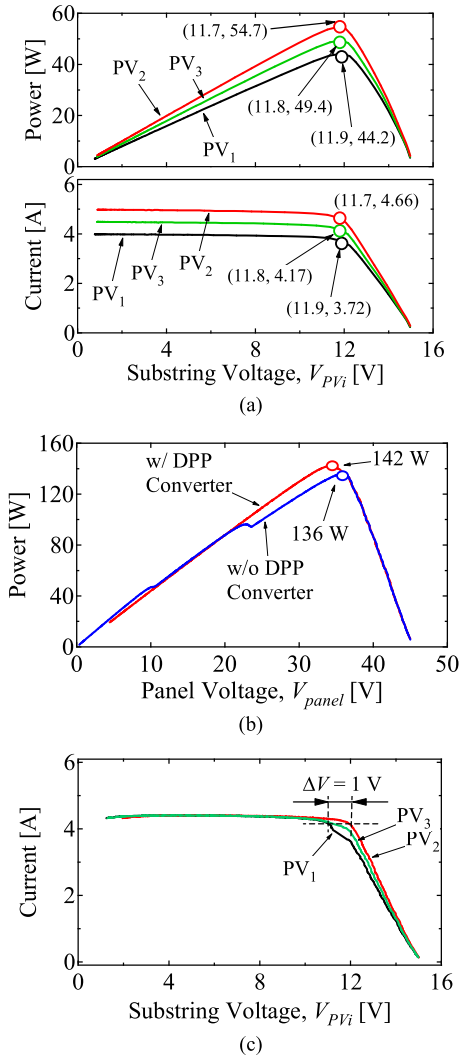

Fig. 15. Experimental results of equalization mode in Case 2. (a) Individual substring characteristics used for the experiment. (b) Measured panel characteristics with/without DPP converter. (c) Substring characteristics equalized by DPP converter.

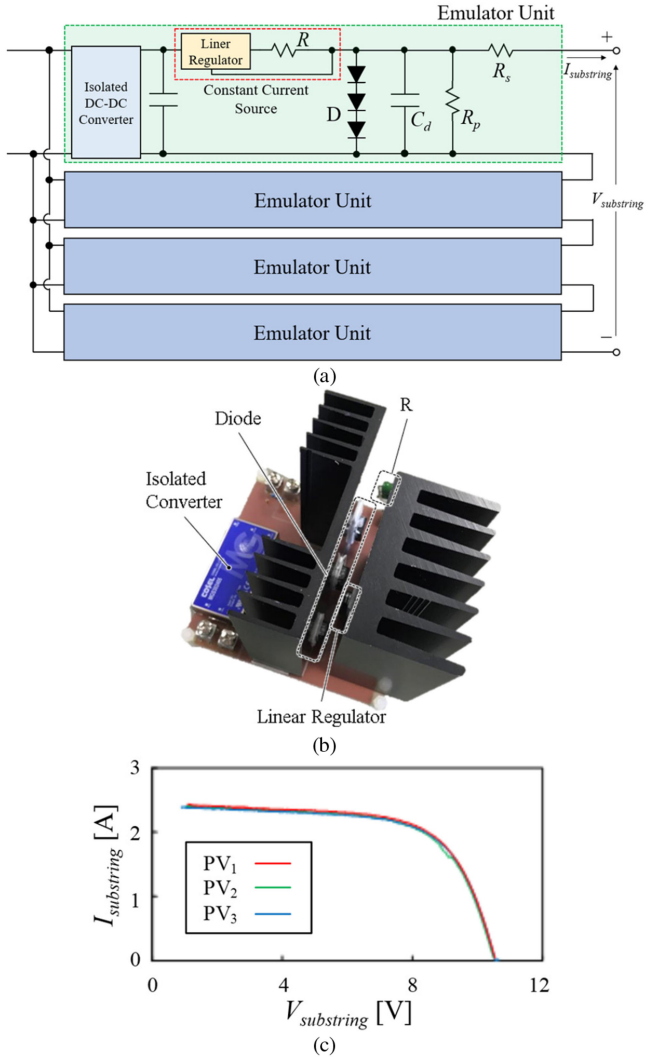

Fig. 16. PV substring emulator. (a) Circuit. (b) Prototype of emulator unit. (c) Measured characteristics of substrings.

TABLE III
COMPONENT LIST OF PV SUBSTRING EMULATOR

Component	Values
R_s	0 Ω
R_p	11 Ω
C_d	Ceramic Capacitor, 1.32 mF
D	Rectifier Diode, BYV29, V_f = 1.03 V
Linier Regulator	LM338T
Isolated Converter	MGS30

shown in Fig. 3(a) were built to ensure the reproducibility of substring characteristics, as shown in Fig. 16. The substring emulator consists of four emulator units, each consisting of R_s, R_p, C_d, three diodes connected in series, and a constant current source. Output ports of four emulator units are connected in series to form a substring emulator.

Components used for the emulator units are listed in Table III. Each emulator unit corresponds to four or five series-connected PV cells, as a total forward voltage drop of three diodes in each emulator unit reaches 3.0 V. The series resistance R_s was removed (i.e., $R_s = 0\ \Omega$) because the emulator units could satisfactorily emulate substring characteristics without R_s. The resistance of the parallel resistor R_p was determined so that the current at the MPP was about 90% of the short circuit current. The previous work reported that C_d of a mono-crystalline silicon PV cell with 125 × 125 mm is approximately 6.0 mF [21]. Since the emulator unit is equivalent to four or five series-connected PV cells, the value of C_d was determined to be 1.32 mF so that C_d is about 1/4 or 1/5 of 6.0 mF. $I-V$ characteristics of the PV substring emulators used for the experimental verification tests are shown in Fig. 16(c).

The prototype was operated with $d_{\text{bias}} = 0.5$ and $\Delta d = 0.05$ to perturb the equalization currents in the frequency range of 10 Hz–10 kHz, while the currents and voltages of the substring emulators were measured using the FRA to obtain Nyquist plots. An electronic load was connected to the panel, and its resistance was adjusted so that the panel operated at its MPP. The values

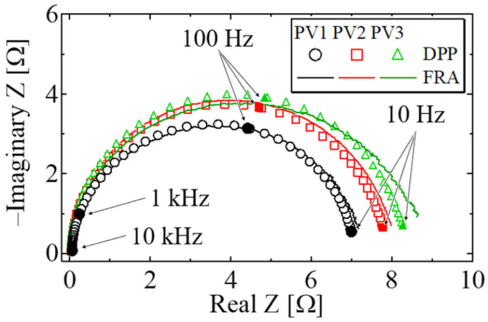

Fig. 17. Measured Nyquist plots.

TABLE IV
CALCULATED PARAMETERS OF PASSIVE ELEMENTS

		DPP Converter	FRA	Error [%]
PV_1	R_s [mΩ]	58.4	55.5	5.23
	R_p [mΩ]	7.34	7.16	2.51
	C_d [μF]	180	172	4.65
PV_2	R_s [mΩ]	36.8	37.2	1.08
	R_p [mΩ]	8.2	7.9	3.80
	C_d [μF]	168	165	1.82
PV_3	R_s [mΩ]	36.5	34.7	5.19
	R_p [mΩ]	7.94	8.35	4.91
	C_d [μF]	173	161	7.45

of R_s, R_p, and C_d were also measured using the FRA alone to compare with the proposed DPP converter.

The Nyquist plots measured with the DPP converter or by the FRA alone are compared in Fig. 17. The frequency range of 10 Hz–10 kHz was sufficient to obtain nearly whole semicircles. Internal parameters of R_s, R_p, and C_d were calculated from the measured Nyquist plots, as shown in Table IV. The results showed good agreement with errors less than several percent. The result demonstrated the efficacy of the ac current perturbation by the proposed panel-to-substring DPP converter.

VI. CONCLUSION

The panel-to-substring DPP converter and its electrical diagnosis technique have been proposed in this article. The proposed DPP converter not only precludes the partial shading issues but also offers the electrical diagnosis capability based on the ac impedance measurement, from which equivalent circuit parameters of PV substrings can be obtained.

The proposed DPP converter operates in either the equalization mode or diagnosis mode. In the equalization mode, the DPP converter operates with the current sensorless ΔV-controlled equalization strategy so that equalization currents from the DPP converter flow toward shaded substrings only. In the diagnosis mode, on the other hand, the DPP converter injects ac equalization currents to all substrings in order to perturbate substring currents.

The experimental equalization tests emulating partial shading conditions for three substrings were performed using the prototype operating with the ΔV-controlled equalization strategy. With the proposed DPP converter, local MPPs successfully disappeared, and the extractable maximum powers significantly increased, demonstrating the enhanced energy yield by the proposed panel-to-substring DPP converter.

In addition, the experimental ac impedance measurement tests using the PV substring emulators were also performed with the prototype of the proposed DPP converter. The substring currents were perturbated by injecting ac equalization currents, and Nyquist plots of three substrings were obtained from the voltage responses to perturbated currents. The equivalent circuit parameters measured with the proposed DPP converter agreed well with those measured by the FRA alone, demonstrating the efficacy of the ac current perturbation by the proposed DPP converter.

REFERENCES

[1] M. Uno, H. Sato, and T. Ishikawa, "Differential power processing converter enhancing energy yield of curved solar roofs of plug-in hybrid electric vehicles," *IEEE Trans. Veh. Technol.*, vol. 69, no. 12, pp. 14689–14700, Dec. 2020.

[2] S. M. MacAlpine, R. W. Erickson, and M. J. Brandemuehl, "Characterization of power optimizer potential to increase energy capture in photovoltaic systems operating under nonuiform conditions," *IEEE Trans. Power Electron.*, vol. 28, no. 6, pp. 2936–2945, Jun. 2013.

[3] M. Vitelli, "On the necessity of joint adoption of both distributed maximum power point tracking and central maximum power point tracking in PV systems," *Prog. Photovolt. Res. Appl.*, vol. 22, pp. 283–299, 2014.

[4] R. C. N. P. Podgurski and D. J. Perreault, "Submodule integrated distributed maximum power point tracking for solar photovoltaic applications," *IEEE Trans. Power Electron.*, vol. 28, no. 6, pp. 2957–2967, Jun. 2013.

[5] H. Jeong, H. Lee, Y. C. Liu, and K. A. Kim, "Review of differential power processing converters techniques for photovoltaic applications," *IEEE Trans. Energy Convers.*, vol. 34, no. 1, pp. 351–360, Mar. 2019.

[6] H. J. Bergveld, *et al.*, "Module-level dc/dc conversion for photovoltaic systems: The delta-conversion concept," *IEEE Trans. Power Electron.*, vol. 28, no. 4, pp. 2005–2013, Apr. 2013.

[7] M. S. Zaman *et al.*, "A cell-level differential power processing IC for concentrating-PV systems with bidirectional hysteretic current-mode control and closed-loop frequency regulation," *IEEE Trans. Power Electron.*, vol. 30, no. 12, pp. 7230–7244, Dec. 2015.

[8] P. S. Shenoy, K. A. Kim, B. B. Johnson, and P. T. Krein, "Differential power processing for increased energy production and reliability of photovoltaic systems," *IEEE Trans. Ind. Power Electron.*, vol. 28, no. 6, pp. 2968–2979, Jun. 2013.

[9] S. Qin, S. T. Cady, A. D. D. García, and R. C. N. Podgurski, "A distributed approach to maximum power point tracking for photovoltaic submodule differential power processing," *IEEE Trans. Power Electron.*, vol. 30, no. 4, pp. 2024–2040, Apr. 2015.

[10] S. Qin, C. B. Barth, and R. C. N. Podgurski, "Enhancing microinverter energy capture with submodule differential power processing," *IEEE Trans. Power Electron.*, vol. 31, no. 5, pp. 3575–3585, May 2016.

[11] F. Wang, T. Zhu, F. Zhuo, and H. Yi, "An improved submodule differential power processing-based PV system with flexible multi-MPPT control," *IEEE J. Emerg. Sel. Top.*, vol. 6, no. 1, pp. 94–102, Mar. 2018.

[12] M. Z. Ramli and Z. Salam, "A simple energy recovery scheme to harvest the energy from shaded photovoltaic modules during partial shading," *IEEE Trans. Power Electron.*, vol. 29, no. 12, pp. 6458–6471, Dec. 2014.

[13] T. Shimizu, O. Hashimoto, and G. Kimura, "A novel high-performance utility-interactive photovoltaic inverter system," *IEEE Trans. Power Electron.*, vol. 18, no. 2, pp. 704–711, Mar. 2003.

[14] T. Shimizu, M. Hirakata, T. Kamezawa, and H. Watanabe, "Generation control circuit for photovoltaic modules," *IEEE Trans. Power Electron.*, vol. 16, no. 3, pp. 293–300, May 2001.

[15] J. T. Stauth, M. D. Seeman, and K. Kesarwani, "Resonant switched-capacitor converters for sub-module distributed photovoltaic power management," *IEEE Trans. Power Electron.*, vol. 28, no. 3, pp. 1189–1198, Mar. 2013.

[16] A. H. Chang, A. T. Avestruz, and S. B. Leeb, "Capacitor-less photovoltaic cell-level power balancing using diffusion charge redistribution," *IEEE Trans. Power Electron.*, vol. 30, no. 2, pp. 537–546, Feb. 2015.

[17] A. Blumenfeld, A. Cervera, and M. M. Peretz, "Enhanced differential power processor for PV systems: Resonant switched-capacitor gyrator converter with local MPPT," *IEEE J. Emerg. Sel. Top. Power Electron.*, vol. 2, no. 4, pp. 883–892, Dec. 2014.
[18] Z. Qiu and K. Sun, "A photovoltaic generation system based on wide voltage-gain DC-DC converter and differential power processors for DC microgrids," *Chin. J. Elect. Eng.*, vol. 3, no. 1, pp. 84–95, Jun. 2017.
[19] M. Gokdaga, M. Akbabab, and O. Gulbudakc, "Switched-capacitor converter for PV modules under partial shading and mismatch conditions," *Sol. Energy*, vol. 170, pp. 723–731, Aug. 2018.
[20] M. Uno and A. Kukita, "PWM converter integrating switched capacitor converter and series-resonant voltage multiplier as equalizers for photovoltaic modules and series-connected energy storage cells for exploration rovers," *IEEE Trans. Power Electron.*, vol. 32, no. 11, pp. 8500–8513, Nov. 2017.
[21] M. Uno, Y. Saito, M. Yamamoto, and S. Urabe, "PWM switched capacitor-based cell-level power balancing converter utilizing diffusion capacitance of photovoltaic cells," *IEEE Trans. Power Electron.*, vol. 34, no. 11, pp. 10675–10687, Nov. 2019.
[22] M. Uno, M. Yamamoto, H. Sato, and S. Oyama, "Modularized differential power processing architecture based on switched capacitor converter to virtually unify mismatched photovoltaic panel characteristics," *IEEE Trans. Power Electron.*, vol. 35, no. 2, pp. 1563–1575, Feb. 2020.
[23] C. Olalla, D. Clement, M. Rodríguez, and D. Makisimović, "Architectures and control of submodule integrated dc-dc converters for photovoltaic applications," *IEEE Trans. Power Electron.*, vol. 28, no. 6, pp. 2980–2997, Jun. 2013.
[24] Y. Levron, D. R. Clement, B. Choi, C. Olalla, and D. Maksimovic, "Control of submodule integrated converters in the isolated-port differential power-processing photovoltaic architecture," *IEEE J. Emerg. Sel. Top. Power Electron.*, vol. 2, no. 4, pp. 821–832, Dec. 2014.
[25] R. Bell and R. C. N. P. Podgurski, "Decoupled and distributed maximum power point tracking of series-connected photovoltaic submodules using differential power processing," *IEEE J. Emerg. Sel. Top. Power Electron.*, vol. 3, no. 4, pp. 881–891, Dec. 2015.
[26] C. Olalla, C. Deline, D. Clement, Y. Levron, M. Rodríguez, and D. Makisimović, "Performance of power limited differential power processing architectures in mismatched PV systems," *IEEE Trans. Power Electron.*, vol. 30, no. 2, pp. 618–631, Feb. 2015.
[27] G. Chu, H. Wen, L. Jiang, Y. Hu, and X. Li, "Bidirectional flyback based isolated-port submodule differential power processing optimizer for photovoltaic applications," *Sol. Energy*, vol. 158, pp. 929–940, Oct. 2017.
[28] Y. T. Jeon, H. Lee, K. A. Kim, and J. H. Park, "Least power point tracking method for photovoltaic differential power processing systems," *IEEE Trans. Power Electron.*, vol. 32, no. 3, pp. 1941–1951, Mar. 2017.
[29] Y. T. Jeon and J. H. Park, "Unit-minimum least power point tracking for the optimization of photovoltaic differential power processing systems," *IEEE Trans. Power Electron.*, vol. 34, no. 1, pp. 311–324, Jan. 2019.
[30] J. Du, R. Xu, X. Chen, Y. Li, and J. Wu, "A novel solar panel optimizer with self-compensation for partial shadow condition," in *Proc. IEEE Appl. Power Electron. Conf. Expo.*, 2013, pp. 92–96.
[31] M. Uno and A. Kukita, "Single-switch voltage equalizer using multi-stacked buck-boost converters for partially-shaded photovoltaic modules," *IEEE Trans. Power Electron.*, vol. 30, no. 6, pp. 3091–3105, Jun. 2015.
[32] M. Uno and A. Kukita, "Current sensorless equalization strategy for a single-switch voltage equalizer using multistacked buck–boost converters for photovoltaic modules under partial shading," *IEEE Trans. Ind. Appl.*, vol. 53, no. 1, pp. 420–429, Jan./Feb. 2017.
[33] M. Uno and A. Kukita, "Two-switch voltage equalizer using an LLC resonant inverter and voltage multiplier for partially-shaded series-connected photovoltaic modules," *IEEE Trans. Ind. Appl.*, vol. 51, no. 2, pp. 1587–1601, Mar./Apr. 2015.
[34] M. Uno and A. Kukita, "Single-switch single-magnetic PWM converter integrating voltage equalizer for partially-shaded photovoltaic modules in standalone applications," *IEEE Trans. Power Electron.*, vol. 33, no. 2, pp. 1259–1270, Feb. 2018.
[35] M. Uno and T. Shinohara, "Module-integrated converter based on cascaded quasi-Z-source inverter with differential power processing capability for photovoltaic panels under partial shading," *IEEE Trans. Power Electron.*, vol. 34, no. 12, pp. 11553–11565, Dec. 2019.
[36] M. Sugiyama, M. Hayashi, C. Yamazaki, N. B. Hamidon, Y. Hirose, and M. Itagaki, "Application of impedance spectroscopy to investigate the electrical properties around the pn interface of Cu(In,Ga)Se_2 solar cells," *Thin Solid Films*, vol. 535, no. 15, pp. 287–290, May 2013.
[37] M. Sugiyama, H. Sakakura, S. W. Chang, and M. Itagaki, "Investigation of sputtering damage around pn interfaces of Cu(In,Ga)Se_2 solar cells by impedance spectroscopy," *Electrochim. Acta*, vol. 131, no. 10, pp. 236–239, Jun. 2014.
[38] K. A. Kim, G. S. Seo, B. H. Cho, and P. T. Krein, "Photovoltaic hot-spot detection for solar panel substrings using AC parameter characterization," *IEEE Trans. Power Electron.*, vol. 31, no. 2, pp. 1121–1130, Feb. 2016.
[39] W. Huang and J. A. A. Qahouq, "An online battery impedance measurement method using DC–DC power converter control," *IEEE Power Electron*, vol. 61, no. 11, pp. 5987–5995, Nov. 2014.
[40] D. A. Howey, P. D. Mitcheson, V. Yufit, G. J. Offer, and N. P. Brandon, "Online measurement of battery impedance using motor controller excitation," *IEEE Tran. Veh. Technol.*, vol. 63, no. 6, pp. 2557–2566, Jun. 2014.
[41] Y. D. Lee, S. Y. Park, and S. B. Han, "Online embedded impedance measurement using high-power battery charger," *IEEE Ind. Appl.*, vol. 51, no. 1, pp. 498–508, Jan./Feb. 2015.
[42] N. Katayama and S. Kogoshi, "Real-time electrochemical impedance diagnosis for fuel cells using a DC–DC converter," *IEEE Energy Convers.*, vol. 30, no. 2, pp. 707–713, Jun. 2015.
[43] E. Din, C. Schaef, K. Moffat, and J. T. Stauth, "A scalable active battery management system with embedded real-time electrochemical impedance spectroscopy," *IEEE Trans. Power Electron.*, vol. 32, no. 7, pp. 5688–5698, Jul. 2017.
[44] C. Schaef, E. Din, and J. T. Stauth, "A hybrid switched-capacitor battery management IC with embedded diagnostics for series-stacked Li–ion arrays," *IEEE J Solid-State Circuit*, vol. 52, no. 12, pp. 3142–3154, Dec. 2017.
[45] W. Wang, A. C. F. Liu, H. S. H. Chung, R. W. H. Lau, J. Zhang, and A. W. L. Lo, "Fault diagnosis of photovoltaic panels using dynamic current–voltage characteristics," *IEEE Trans. Power Electron.*, vol. 31, no. 2, pp. 1588–1599, Feb. 2016.
[46] K. A. Kim, P. S. Shenoy, and P. T. Krein, "Converter rating analysis for photovoltaic differential power processing systems," *IEEE Trans. Ind. Electron.*, vol. 30, no. 4, pp. 1987–1997, Apr. 2015.
[47] C. Olalla, M. N. Hasan, C. Deline, and D. Maksimovi, "Mitigation of hot-spots in photovoltaic systems using distributed power electronics," *Energies*, vol. 11, Mar. 2018, Art. no. 726.

Masatoshi Uno (Member, IEEE) was born in Japan in 1979. He received the B.E. degree in electronics engineering and the M.E. degree in electrical engineering from Doshisha University, Kyoto, Japan, in 2002 and 2004, respectively, and the Ph.D. degree in space and astronautical science from the Graduate University for Advanced Studies, Hayama, Japan, in 2012.

In 2004, he joined the Japan Aerospace Exploration Agency, Sagamihara, Japan, where he developed spacecraft power systems including battery, photovoltaic, and fuel cell systems. In 2014, he joined the Department of Electrical and Electronics Engineering, Ibaraki University, Ibaraki, Japan, where he is currently an Associate Professor of Electrical Engineering. His research interests include switching power converters for renewable energy systems, life evaluation for EDLCs and lithium-ion batteries, and development of spacecraft power systems.

Dr. Uno was the recipient of the Isao Takahashi Power Electronics Award in 2018.

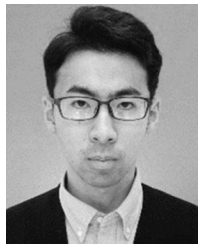

Kazuma Honda was born in Japan in 1996. He received the B.E. and M.E. degrees in electrical engineering from Ibaraki University, Ibaraki, Japan, in 2019 and 2021, respectively.

Since 2021, he has been with Hitachi Industrial Products Ltd, Tokyo, Japan. His research interests include differential power processing converters for photovoltaic systems.